



Synthesis of xanthan gum/trimethyl chitosan interpolyelectrolyte complex as pH-sensitive protein carrier

Mahmoud H. Abu Elella¹ · Demiana H. Hanna¹ · Riham R. Mohamed¹ · Magdy W. Sabaa¹

Received: 1 December 2020 / Revised: 2 March 2021 / Accepted: 4 March 2021 /
Published online: 12 March 2021

© The Author(s), under exclusive licence to Springer-Verlag GmbH Germany, part of Springer Nature 2021

Abstract

Protein delivery journey through gastrointestinal (GI) tract faces many challenges due to its physicochemical instabilities, fugitive half-life, and less absorption efficiency. Herein, the aim is the study of both the encapsulation and in-vitro-release of the bovine serum albumin (BSA) through pHs of GI tract within the green synthesized interpolyelectrolyte complex, which was prepared from biodegradable polymers as XG and TMC-based highly an efficient pH-sensitive protein carrier to solve the drawbacks of the protein delivery through GI tract. The structures of XG/TMC PEC and BSA-loaded PEC were elucidated using different analysis tools like FTIR, FE-SEM, EDX, and XRD techniques. The BSA-loaded and released profiles were determined in pH 1.2 (gastric simulated pH) and pH 7.4 (intestine simulated pH) media. Best BSA-loaded results were obtained with the increase in XG concentration, BSA-loaded concentration, and encapsulation time. Moreover, in vitro BSA release results showed that the amount of BSA released in pH 7.4 was higher than that in pH 1.2 and also went up with the rise within the amount from 12 to 120 h to be 97.9% in pH 7.4 and 29.7% in pH 1.2 at 120 h. Moreover, according to SDS-PAGE technique, the BSA was released in intact form out of the PECs; thus, the encapsulation and released conditions did not affect the structural integrity of BSA structure. Finally, the cytotoxicity study of the prepared PEC showed safe and good biocompatibility properties against the traditional human melanocyte cell line.

Keywords Protein delivery · Interpolyelectrolyte complex · Bovine serum albumin · Cytotoxicity

✉ Mahmoud H. Abu Elella
mahmoudhussien3766@yahoo.com

¹ Chemistry Department, Faculty of Science, Cairo University, Giza 12613, Egypt

Introduction

The biggest problem of protein, in its journey through gastrointestinal (GI) tract, is its instability, short half-life, and its degradation in the stomach [1]. Also, protein injection leads to some problems such as fat deposits at injection sites, local infection, protein resistance, and stress which lead to poor compliance, non-effective treatment, and patient discomfort [2, 3]. Thus, numerous efforts have been exerted to discover highly efficient carriers for oral delivery of protein due to its convenience and patient compliance in short- and long-term treatment [4, 5].

Consequently, synthesis of stimuli-responsive hydrogels based on biodegradable polymers as polysaccharides have great attention for many global research groups to solve the previously mentioned problems due to their non-toxicity, excellent biocompatibility and biodegradability. So, they have high selectivity for drugs (protein) delivery since they are capable of changing their characteristics as exposed to external environmental conditions such as pH, temperature, and light [6–8].

Xanthan gum, XG is an anionic biodegradable polysaccharide gum which is excreted from *Xanthomonas campestris* (Gram-negative bacterium). XG structure is shown in Fig. 1a. XG is a natural anionic antioxidant biopolymer that is used widely today through several industries like biomedical, food, pharmaceuticals, textile, cosmetics, and petrochemical industries due to its biocompatibility, biodegradability, thermally stability, and non-toxicity. However, some drawbacks can reduce the potential uses of XG in industrial applications like the chance of its microorganism contamination where it can be degraded by microbial attack [9–15].

Chitosan (Ch) is a modified biodegradable natural copolymer polysaccharide having polycationic nature. Ch is prepared via partially alkaline deacetylation hydrolysis reaction at high temperature for *N*-acetamide units of chitin structure. Ch dissolved in acidic medium only, so it has limited applications. Consequently, it has been chemically modified into water-soluble derivatives including *N*-quaternized derivatives which have a permanent positive charge on their backbone. Trimethyl chitosan chloride, TMC, Fig. 1b, is a water-soluble quaternized derivative as it dissolves over

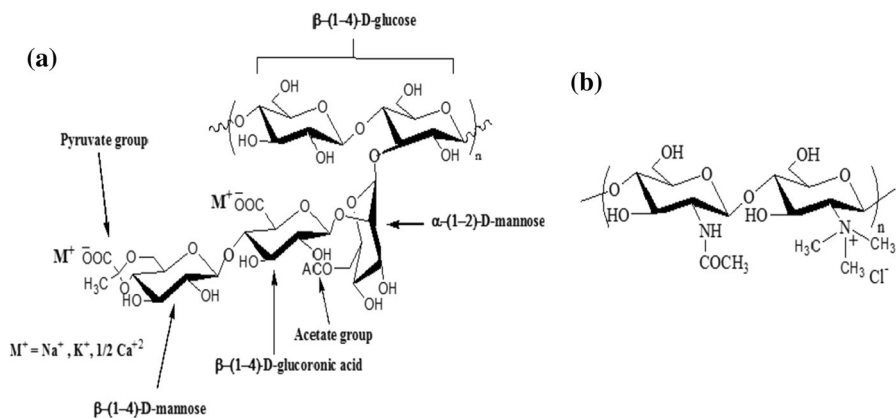


Fig. 1 Chemical structure of **a** XG and **b** TMC

broad pH range (2–9). TMC improves both solubility and antibacterial activity of Ch. TMC is used widely in several applications: biomedical, food additives, antimicrobial agents, and pharmaceuticals due to its excellent properties: biocompatibility, thermal stability, biodegradability, antimicrobial activity, non-toxicity, antioxidant activity and anti-inflammatory properties [16–21]. Thus, we expect that complexing XG with TMC through strong inter electrostatic interactions (Coulomb's interactions) will encapsulate BSA in a good manner.

Chemicals and experimental methods

Chemicals

Chitosan (DD=90–95% and Average Mwt= 16×10^4 gmol⁻¹) was purchased from Oxford Laboratory, India. Xanthan gum (Average Mwt is 17×10^5 gmol⁻¹ and pKa value is 4.6) was obtained from Alpha-Chemika, India. Dimethyl sulfate (CH₃)₂SO₄ and buffered saline solutions were purchased from Loba Chemie Pvt. Ltd., Mumbai, India. NaCl, absolute ethanol, and NaOH were supplied by Merck (Schuchardt OHG) Hohenbrunn, Germany. Bovine serum albumin (BSA) and coomassie Brilliant Blue G-250 were provided from Sigma-Aldrich, Germany. Regenerated cellophane dialysis tubes (Average Mwt: $12\text{--}14 \times 10^3$ gmol⁻¹) were obtained from Serva Electrophoresis, Heidelberg, Germany.

Experimental methods

Synthesis of trimethyl chitosan chloride

Trimethyl chitosan chloride, TMC, was synthesized according to Britto method [22]. Briefly, 1.0 g of Ch was soaked in (CH₃)₂SO₄ (16 mL) and dist.H₂O (4 mL) for 3 h, then 0.5 g of NaOH and 0.4 g of NaCl were added through 30 min under continuous stirring which continued for another 6 h at 30 °C. Then, the product was purified by dialysis tubes using dist.H₂O for 3 days, after that it was precipitated in 600 mL cold absolute ethanol and washed by diethyl ether. The final product (TMC) was collected with centrifugation (4000 rpm) for 15 min and dried under vacuum at 40 °C.

Encapsulation of BSA within XG/TMC PECs

BSA was chosen as a protein model, to study the protein loading and release property within XG/TMC PECs. Both BSA loading and encapsulation efficiency percent, %DL and % EE, respectively) was investigated according to Bradford method [23]. Briefly, XG (0.1 g, 0.001 mol.) was soaked in 40 mL of dist. water under stirring for 15 min. Next, a definite weight of BSA was dissolved in 20 mL dist. water, and then it was dispersed in the above XG solution. Then, TMC (0.1 g, 0.004 mol.) was dissolved in 40 mL dist. water then was added dropwisely to the above mixture

under constant stirring for 24 h at room temperature (~30 °C). After that, precipitated BSA-loaded PECs were collected using centrifugation (3000 rpm), and then were dried in vacuum oven at 40 °C for 24 h till constant weight. While the PECs in the absence of BSA were prepared as a control by the same above method. BSA encapsulation was examined under the effect of different parameters such as:

1. XG: TMC weight ratios which are 1:1, 1:2, and 2:1;
2. Different loaded BSA concentrations: 25–75 (wt/wt %);
3. Encapsulation time: 3–24 h.

Determination of encapsulation efficiency of BSA

The encapsulation efficiency (EE) % and drug loading (DL) % of BSA in the interpolyelectrolyte complexes (XG/TMC PECs) were determined by Bradford method [23]. Firstly, BSA-loaded PECs (10 mg) was dissolved in 10 mL of an aqueous phase mixture, which was composed from 1 mL of benzyl alcohol and 9 mL of dist. water, and then were shaken for a definite time (12 h) to get BSA out of PECs matrix into an aqueous phase. Above all, the samples were centrifuged at (2000 rpm), and finally, the BSA concentration was estimated using Coomassie brilliant blue G250 protein assay, whereas the prepared unloaded PECs supernatant solution (in the absence of BSA) was used as a blank to calculate the both % DL and % EE according to the following below Eqs. (1) and (2) [24].

$$\% \text{ DL} = [(W_2 - W_3) / W_1] \times 100 \quad (1)$$

$$\% \text{ EE} = [(W_2 - W_3) / W_2] \times 100 \quad (2)$$

where W_1 is weight of the purified unloaded PECs samples, which obtained after washing them by dist. water for three times to remove unreacted materials, and then dried in vacuum oven at 40 °C for 24 h till constant weight. While, W_2 , and W_3 are weights of total amount of BSA, and free BSA in the supernatant, respectively. The compositions of XG/BSA/TMC matrices are given in Table 1.

Table 1 Composition of loaded BSA within PECs under various parameters

Factors Sample code	Weight ratios (%w/w) (XG/ TMC)	BSA-loaded concentration (%w/w)	BSA-loaded PECs formation time (h)
P1	1:1	25%	24
P2	2:1	25%	24
P3	1:2	25%	24
P4	1:1	50%	24
P5	1:1	75%	24
P6	1:1	25%	3
P7	1:1	25%	6
P8	1:1	25%	12

Kinetic swell ability studies of unloaded PECs

Kinetic studies of swell ability for unloaded PECs (in absence of BSA) in both pH 7.4 and 1.2 (phosphate buffered saline solutions) were studied through various time intervals from 0.5 to 6 h at 37 °C. Briefly, 0.1 g of unloaded PECs (W_i) was immersed in 50 mL PBS through different time intervals from 0.5 to 6 h at 37 °C till reaching equilibrium. The excess water was removed from swelled sample surfaces with filter paper then they were weighed (W_F). The swell ability % was calculated according to Eq. (3) [24, 25].

$$\text{Swell ability \%} = [(W_F - W_i)/W_i] \times 100 \quad (3)$$

where W_F and W_i are the swollen and dry PECs weights, respectively.

In vitro release of BSA

In vitro BSA released from XG/BSA/TMC matrices was studied in pH 1.2 and 7.4 and evaluated using Coomassie brilliant blue G250 protein assay [23]. Briefly, a definite weight of the prepared BSA-loaded PECs (100 mg) was soaked in a conical flask having 8 mL of released buffered medium under shaking incubator (70 rpm) at 37 °C for various time intervals: 12, 24, 48, 72, and 120 h. After released time, BSA-loaded samples were centrifuged at 2000 rpm then 4 mL of the supernatant was gathered from the released buffer medium to estimate BSA concentration using Coomassie brilliant blue G250 protein assay. The same amount of fresh released buffered medium (4 mL) was added—instead of the taken amount—to keep the original volume constant. The BSA cumulative release % was determined using Eq. (4) [24, 26].

$$\text{The BSA cumulative release \%} = (C_A/C_i) \times 100 \quad (4)$$

where C_A and C_i are the weights of supernatant and initial BSA solution, respectively.

All experimental works were done three times and the mean values were calculated.

Kinetic studies of BSA release

Kinetic *in vitro* BSA release from XG/BSA/TMC matrices was studied by Koresmeyer model according to a diffusion exponent (n) which can be calculated using Eq. (5) [27–29].

$$M_t/M_\infty = K t^n \quad (5)$$

where M_t and M_∞ are the released weights of BSA at different time intervals (t) and infinite time (120 h), respectively. k and n are constant and diffusion exponent, respectively. The mechanism of BSA release from loaded PECs matrices

depends on n values: $n = 0.45$ – 0.5 (Fickian or diffusion-controlled release model), $n = 0.5$ – 0.89 (non-Fickian or diffusion and erosion-controlled release model), $n = 0.89$ – 1.0 (Case II transport model), and $n > 1.0$ (Super case II transport).

Polyacrylamide gel electrophoresis studies

The structure of released BSA from loaded PECs was lyophilized and reconstituted in PBS, then checked with sodium dodecyl sulfate–polyacrylamide gel electrophoresis, SDS-PAGE, as mentioned in Laemmli method [30]. The prepared samples (the molecular marker, standard BSA, and released BSA from the loaded hydrogels) were separated by SDS-PAGE technique in a 4% stacking gel, 1.5 mm thick, and 12% resolving gel. The electrophoresis was done with Protean II vertical electrophoresis cell, Bio-Rad, at 200 V, and the bands were visualized by Coomassie blue staining.

Cytotoxicity (Cell compatibility) assay

Cytotoxicity assay of unloaded PECs was examined against HFB-4, normal human melanocytes cells, by a neutral red uptake assay test, NRU [31]. The absorbance of acidified ethanol solution including extracted neutral red dye with a microplate reader (BioTek, ELX808) was measured at 540 nm to estimate the optical density (OD), then cell viability was calculated according to Eq. (6).

$$\text{Cell viability \%} = \left[1 - \left(\text{OD}_{\text{tested}} / \text{OD}_{\text{control}} \right) \right] \times 100 \quad (6)$$

where $\text{OD}_{\text{tested}}$ is the optical density of wells which were treated with PEC samples and $\text{OD}_{\text{control}}$ is the optical density of controlled cell lines.

Characterization (Instrumentation)

The TMC structure was elucidated using Proton Nuclear Magnetic Resonance ($^1\text{H-NMR}$, Varian Mercury (VX-300) NMR) spectroscopy and compared to unmodified Ch. $^1\text{H-NMR}$ spectra were run at 300 MHz in DMSO/trichloroacetic acid (TFA) and D_2O as solvents for Ch and TMC, respectively.

The chemical structure of tested samples was elucidated using Fourier Transform Infrared (FTIR, Jasco FTIR 4100 spectrometer, Japan) spectroscopy within wave number range 4000 to 600 cm^{-1} at 25 °C.

The surface morphology of samples was investigated using field emission scanning electron microscope (FE-SEM, Quanta 250 FEG, FEI Company, Netherland) with a magnification (X 1000). A strip of sample was placed on the carbon tape on a stub and was coated with Au. In addition, the elemental analysis of tested samples was examined via energy dispersive x-ray (EDX) unit which is attached with FE-SEM technique.

The structure crystallinity of tested samples was investigated using X-Ray diffractometry (XRD) (Philips Xpert MPD Pro) using Ni-filter and Cu K α radiation source at an accelerating voltage (50 kV) and current (40 mA).

The structural integrity of released BSA from loaded PECs matrices was examined using vertical sodium dodecyl sulfate–polyacrylamide gel electrophoresis apparatus (a Protean II vertical electrophoresis cell (Bio-Rad)).

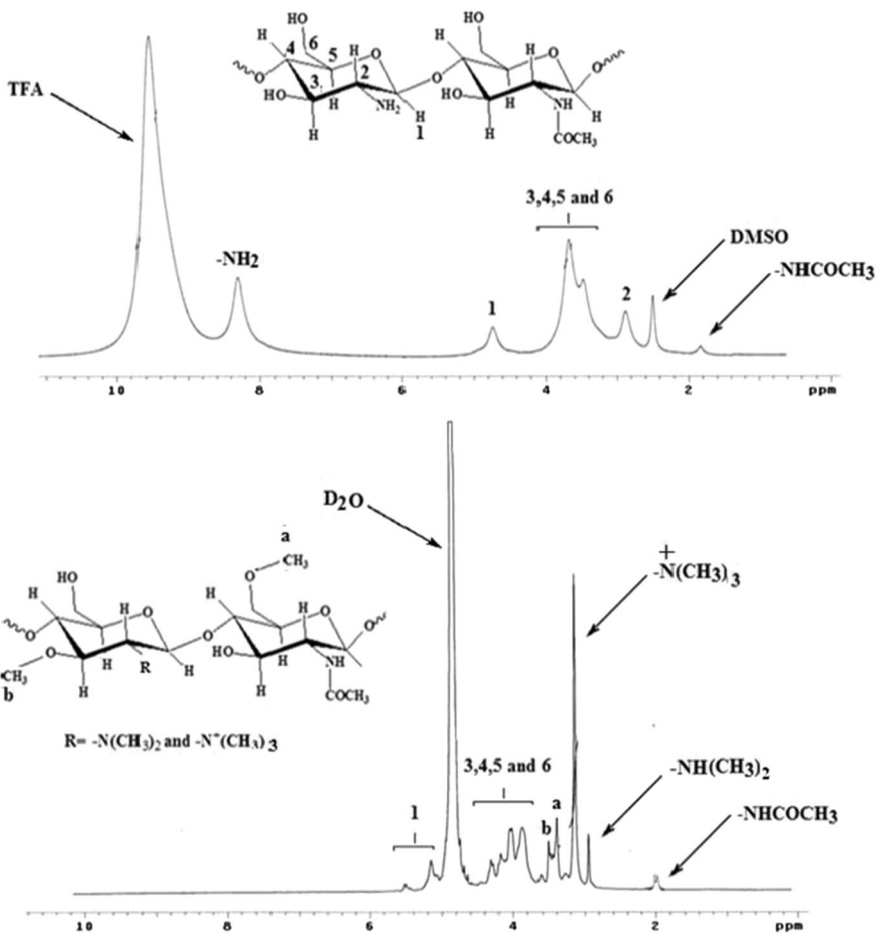


Fig.2. ¹H-NMR spectra of Ch and TMC structure

Results and discussion

Characterization of TMC- and BSA-loaded PEC

1. Proton nuclear magnetic resonance spectroscopy

The chemical structure of prepared TMC was been essentially elucidated with ^1H -NMR spectroscopy and compared with unmodified Ch as shown in Fig. 2. ^1H -NMR spectrum of the native Ch shows singlet signals at 1.8 ppm, 2.8 ppm, 4.7 ppm, and 8.3 ppm, which refer to the protons that present in the *N*-acetyl groups; both *N*-glucosamine and *N*-acetyl glucosamine units that bonded to C2; anomeric proton [H_1] of glycopyranose unit; and protons of primary amino groups, respectively. Additionally, a multiplet signal appeared at $\delta=3.5\text{--}3.8$ ppm indicated to the four protons, $\text{H}_3, \text{H}_4, \text{H}_5$ and H_6 , attached to C3, C4, C5, and C6, respectively [22, 32–35]. Moreover, two singlet signals situated at 2.5 ppm and 9.6 ppm referred to DMSO and TFA solvents which are used for dissolving Ch.

On the other hand, ^1H -NMR spectrum of TMC revealed five singlet signals: at $\delta=2.0$ ppm corresponded to protons of methyl group in remaining *N*-acetyl groups; at $\delta=3.0$ ppm referred to protons of *N*-dimethyl amino ($-\text{N}(\text{CH}_3)_2$) groups; at $\delta=3.2$ ppm signed for protons of *N*-quaternized amino ($-\text{N}(\text{CH}_3)_3$) groups; and two signals at $\delta=3.35$ ppm and 3.47 ppm corresponded to protons of methyl group that connected to oxygen atom that attached to carbon atom 6 ($\text{O}^6\text{--CH}_3$) and 3 ($\text{O}^3\text{--CH}_3$), respectively [22, 35]. In addition to appear multiplet signals at $\delta=3.8\text{--}4.4$ and 5.0–5.4 ppm signed for protons attached to carbon atoms 3, 4, 5 and 6 [$\text{H}_3, \text{H}_4, \text{H}_5$ and H_6] and anomeric proton [H_1], respectively [22, 35, 36]. Also, sharp singlet signal appeared at $\delta=4.8$ ppm related to D_2O solvent for TMC. Additionally, the degree of quaternization (DQ) % in TMC structure was determined according to Eq. (7).

$$\text{DQ \%} = \left[\frac{[(-\text{N}^+(\text{CH}_3)_3)]}{(9 \times [\text{H}_1])} \right] \times 100 \quad (7)$$

where $[(-\text{N}^+(\text{CH}_3)_3)]$ corresponded to the integral area of *N*-quaternized protons signal at 3.2 ppm; and 9 number is the number of *N*-quaternized protons; and [H_1] signed for the integral area of anomeric proton signal at $\delta=5.0\text{--}5.4$ ppm [35]. % DQ in TMC structure was calculated as 46.6%.

2. Fourier transform infrared spectroscopy

Chemical structure of all examined samples: Ch, TMC, XG, PEC (XG/TMC (1:1); in the absence of BSA), BSA, and BSA-loaded PEC (BSA/PEC, P1) was elucidated by Fourier Transform Infrared, FTIR, spectroscopy, and the results are shown in Fig. 3a, b. Ch FTIR spectrum showed a broad absorption peak at 3490 cm^{-1} related to $-\text{OH}$ and $-\text{NH}_2$ groups stretching vibrations, strong two absorption peaks at 1645 and 1386 cm^{-1} referred to asymmetric and symmetric amide groups stretching vibration and two absorption peaks at 1105 and 1013 cm^{-1} assigned for second and first alcoholic (C--OH) groups stretching vibration [37]. While TMC spectrum

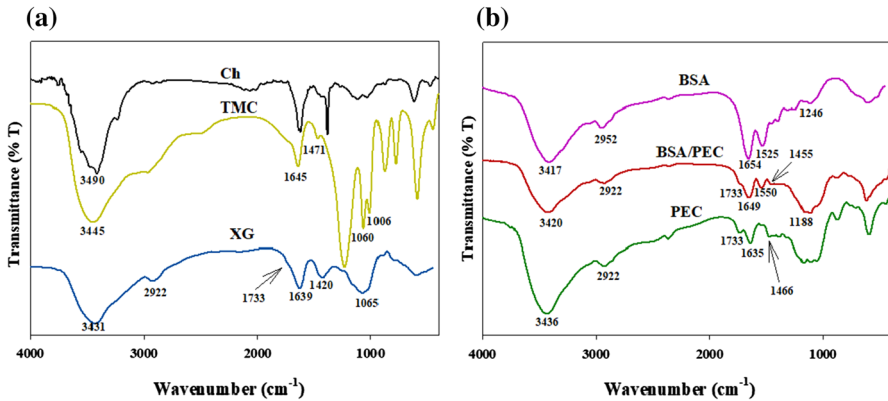


Fig. 3 FTIR spectra of **a** XG, Ch, TMC and **b** BSA, PEC (XG/TMC (1:1); in the absence of BSA), and BSA-loaded PEC (BSA/PEC, P1)

showed some changes in the absorption peaks of Ch such as the appearance of –OH groups stretching vibration peak at 3445 cm⁻¹ with less intensity than that found in Ch spectrum at 3490 cm⁻¹ because the amino groups in Ch are converted to *N*-methylated amino groups on TMC chains. Additionally, the two peaks of second and first alcoholic (C–OH) groups stretching vibration appeared at 1060 and 1006 cm⁻¹ due to O-methylation reaction on them. Moreover, the appearance of a new absorption peak at 1471 cm⁻¹ related to the bending vibration of *N*-quaternized amino groups on TMC chains [22, 38–40]. Moreover, FTIR spectrum of XG showed broad peak related to –OH groups stretching vibration at 3431 cm⁻¹, absorption peak referred to stretching vibration of aliphatic –CH groups at 2920 cm⁻¹, the peak of carbonyl group appeared at 1733 cm⁻¹, two absorption peaks assigned for asymmetric and symmetric stretching vibrations of carboxylate groups at 1639 and 1420 cm⁻¹, respectively, and a broad absorption peak of glycosidic ether bond (C–O–C) appeared at 1065 cm⁻¹ [41, 42].

On the other hand, Fig. 3b shows FTIR spectra of unloaded PEC (XG/TMC (1:1); in the absence of BSA), BSA, and BSA/PEC (P1) matrix. PEC spectrum illustrated all characteristic peaks of both XG and TMC with some changes such as a broader –OH group peak at 3436 cm⁻¹ than that found in native XG due to the intermolecular hydrogen bonding interactions between –OH groups in XG chains and *N*-methylated groups on TMC. Moreover, shifted the carboxylate groups peaks in XG to 1635 and 1412 cm⁻¹, and the *N*-methylated groups peak on TMC to 1466 cm⁻¹, due to the electrostatic interactions between carboxylate groups in XG and *N*-quaternized groups on TMC chains.

FTIR spectrum of PEC proved the interaction between XG and TMC via both electrostatic and H-bonding interactions. Additionally, BSA (protein) spectrum showed stretching vibration broad peak for carboxylic and amino groups at 3417 cm⁻¹, the aliphatic –CH groups peak appeared at 2952 cm⁻¹, the absorption peak of carbonyl (amide I) group appeared at 1654 cm⁻¹, the absorption peak of secondary amine (amide II) group appeared at 1525 cm⁻¹, and absorption peak of

amide III groups was detected at 1246 cm^{-1} [43]. Meanwhile, BSA-loaded PEC spectrum showed all characteristic peaks of XG, TMC, and BSA peaks with some changes such as the two absorption peaks of -OH groups along the XG structure (which was mentioned previously in Fig. 3a at 3431 cm^{-1}) and of both carboxylic and amino groups in BSA structure (which was mentioned also previously in Fig. 3b at 3417 cm^{-1}) shifted to appear at 3420 cm^{-1} but less intense and broader than that found in both XG/TMC PEC (in the absence of BSA) and BSA spectra may be because of the H-bonding interactions in BSA/PEC matrix. Moreover, the bending vibration peak of N-quaternized amino groups along the TMC structure more shifted than that found in unloaded PEC, it showed at 1455 cm^{-1} may be due to the strong electrostatic interactions with the carboxylate groups over both XG and BSA structures. And also, shifting for the carboxylate group peak in XG and the amide I peak in BSA to 1649 cm^{-1} owing to both interaction bonds (H-bonding and electrostatic interactions). Finally, the secondary amine peak in BSA shifted from 1525 to 1550 cm^{-1} ; as a result, the electrostatic interactions with carboxylate groups along the XG structure. Consequently, FTIR spectrum of BSA-loaded PEC supported that the encapsulation of BSA inside PEC occurred successfully.

3. Field emission scanning electron microscope

Surface morphology of examined samples: Ch, TMC, XG, PEC (XG/TMC (1:1); in the absence of BSA), BSA, and BSA-loaded PEC (BSA/PEC, P1) was investigated by field emission scanning electron microscope (FE-SEM) technique and microstructure images are shown in Fig. 4. Ch has compact and regular surface due to the intermolecular H-bonding interactions [32] while TMC surface was covered with lumps and aggregations due to the extensive formation of methyl bulky groups on its surface leading to destruction of H-bonds in Ch chains. While XG and BSA surface exhibited irregular lobules [41, 43]. On the other hand, the surface morphology of PEC and BSA / PEC matrix was scanned in two different magnifications; X 1000 and X 2000. PEC surface showed heterogeneous rough surface with pores and cavities filled and covered with small white particles in FE-SEM images of BSA that proved successful encapsulation and loading of PEC with BSA.

4. X-ray diffraction

The crystallinity of examined samples: Ch, TMC, XG, BSA, PEC (XG/TMC (1:1); in the absence of BSA), and loaded PEC (BSA/PEC, P1) was examined via X-ray diffraction technique, XRD, and their patterns are illustrated in Fig. 5a, b. XRD diffractogram of Ch showed two strong diffraction peaks at $2\theta=9.5^\circ$ and 20.0° indicating its crystalline nature due to the intermolecular H-bonding interactions among its chains [37]. After the methylation of Ch, TMC diffractogram exhibited less intense broad diffraction peak at $2\theta=20.0^\circ$ than that found in Ch pattern due to the destruction of the intermolecular H-bonding interactions in Ch. XRD pattern of XG illustrated one weak peak at $2\theta=20^\circ$ indicating its amorphous nature [44]. Meanwhile, the XRD pattern of XG/TMC PEC in the absence of BSA (Fig. 5b) showed one broader peak than that in both TMC and XG patterns individually at $2\theta=20.5^\circ$

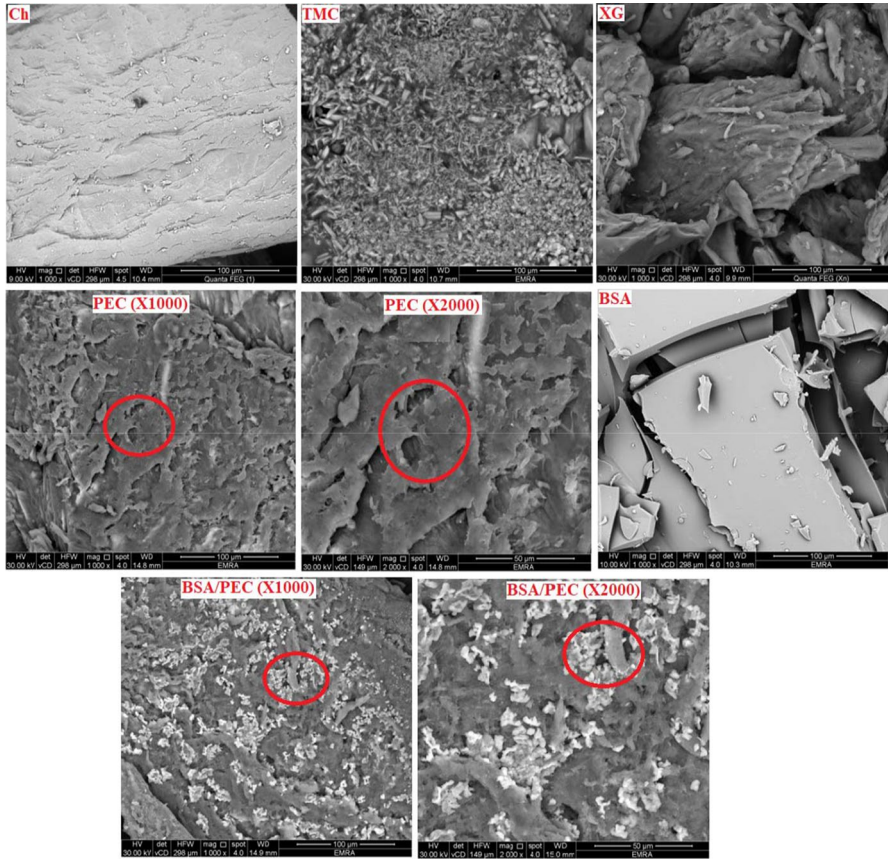


Fig. 4 FE-SEM images of tested samples: XG, Ch, TMC, BSA, PEC (XG/TMC (1:1); in the absence of BSA), and BSA-loaded PEC (BSA/PEC, P1)

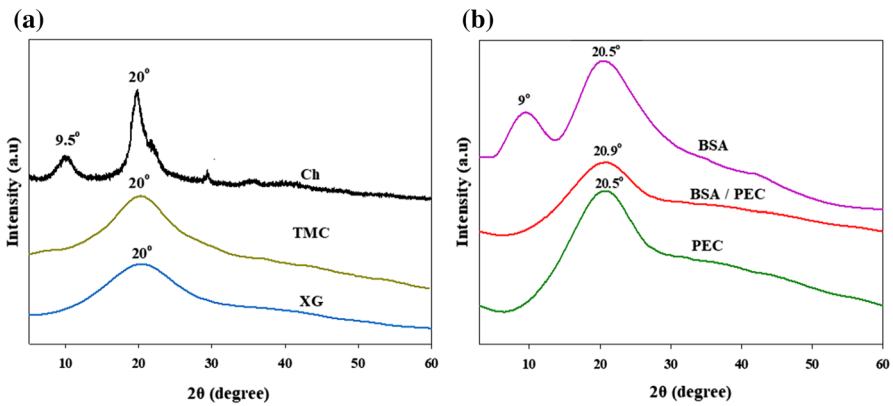


Fig. 5 XRD diffraction patterns of **a** TMC, Ch, XG and **b** BSA, PEC (XG/TMC (1:1); in the absence of BSA), BSA-loaded PEC (BSA/PEC, P1)

which supported the fact of interpolyelectrolyte complex formation between XG and TMC successfully. In addition, BSA XRD pattern showed two broad strong diffraction peaks at $2\theta=9^\circ$ and 20.5° indicated its crystalline nature due to presence of hydrogen bonding interactions among BSA chains [23]. Finally, BSA-loaded PEC pattern exhibited one broad peak at $2\theta=20.9^\circ$ which is less intense than that found in PEC pattern. Also, the disappearance of the diffraction peak of BSA at $2\theta=9^\circ$ proved the homogenous distribution of BSA among PEC chains.

5. Elemental analyses

Elemental composition of XG, TMC, PEC (XG/TMC (1:1); in the absence of BSA), BSA, and BSA-loaded PEC (BSA/PEC, P1) matrix was performed on the EDX unit, and the results are shown in Fig. 6. XG spectrum was reported previously by the same authors [43]. It showed four peaks at 0.280, 0.530, 1.04, and 3.71 keV signed for four elements C, O, Na, and Ca, respectively, while TMC spectrum exhibited four EDX peaks at 0.285, 0.380, 0.533, and 2.70 keV referred to four elements C, N, O, and Cl, respectively. The presence of Cl peak corresponded to *N*-quaternized amino groups onto TMC chains, while PEC hydrogel spectrum showed five peaks at 0.270, 0.371, 0.520, 1.03, and 2.65 keV referring to five elements C, N, O, Na, and Cl, respectively. However, the Na peak intensity was less than that in XG spectrum.

In addition, the peak of Ca element vanished in PEC spectrum and the intensity of the Cl peak decreased than that in TMC spectrum indicating successful synthesis of PEC hydrogels between XG and TMC via electrostatic interactions. Besides, EDX spectrum of BSA was previously discussed by the same authors [43]. It exhibited

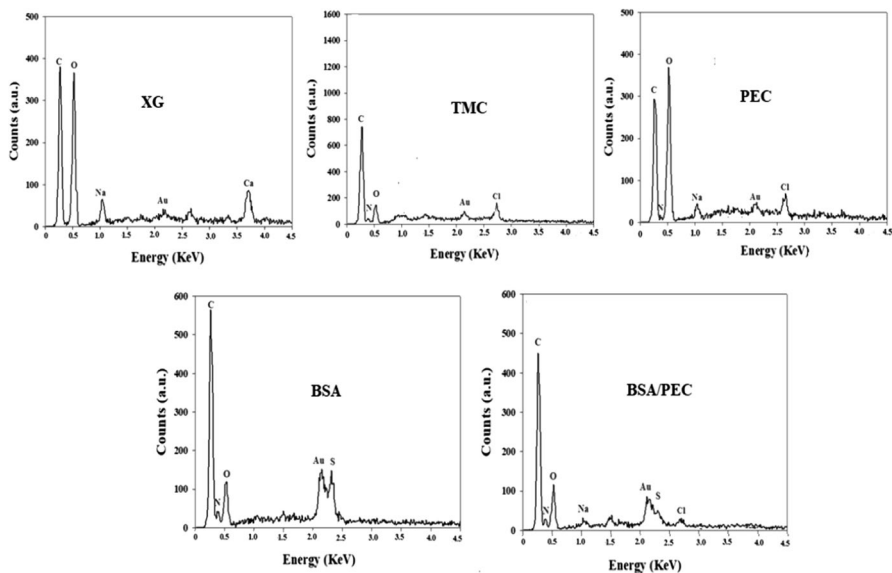


Fig. 6 EDX spectra of TMC, XG, PEC (XG/TMC (1:1); in the absence of BSA), BSA, and BSA-loaded PEC (BSA/PEC, P1)

four peaks at 0.274, 0.390, 0.538, and 2.316 keV referred to four different elements such as C, N, O, and S, respectively. The EDX spectrum of BSA was similar to others that reported in the literature [45, 46]. However, BSA-loaded PEC matrix spectrum illustrated six peaks at 0.270, 0.381, 0.533, 1.03, 2.323, and 2.756 keV referring to six different elements: C, N, O, Na, S, and Cl, respectively. The appearance of S peak in BSA-loaded PEC spectrum proved the successful encapsulation of BSA within PEC. Also, Cl peak intensity was less than that in TMC and PEC spectra which indicated successful encapsulation of BSA within PEC hydrogel through electrostatic interactions. Furthermore, the gold (Au) peak is observed in EDX spectra due to coating the samples with Au before their examination onto FE-SEM technique.

Loading efficiency of BSA

Potential loading of BSA within PEC (XG/TMC) was investigated using different parameters such as; (XG: TMC) weight ratios: (1:1), (2:1), and (1:2) and their codes were P1, P2, and P3, respectively. Also, various BSA concentrations: 75, 50 and 25% w/w% of total XG/TMC weight with codes P5, P4 and P1, respectively. Besides, encapsulation time (3, 6, 12, and 24 h) with codes P6, P7, P8 and P1, respectively. All those parameters affected the percentage of drug (BSA) loading (% DL) and encapsulation efficiency (% EE), the results are shown in Table 2.

(TMC: XG) (2: 1) (P3) was formed via electrostatic interactions between TMC (N-quaternized amino groups) and BSA (carboxylic acid groups). When all the other parameters were kept constant ([BSA]=25% (w/w) and encapsulation time was 24 h), both % DL and % EE increased to give maximum values 15.72% and 80.1% with the increase in TMC content. This observation is similar to previous reported data in the literature [47]. (TMC: XG) (1:1) was formed and encapsulation time was 24 h, % DL and % EE increased to 52% and 91.70% with the increase in BSA concentration 75% (%w/w) due to the increase in BSA concentration which led to raising the interaction between PECs and BSA through electrostatic interactions forces which increases the amount of BSA loaded within PECs hydrogels. The obtained results are similar to the previously reported data in the literature [47, 48].

Table 2 BSA loading % and encapsulation efficiency %

Parameters	Code of sample	BSA loading %	Encapsulation efficiency %
Polymer weight ratios (%w/w)	P1	15.38 ± 0.02	77.0 ± 0.03
	P2	15.20 ± 0.01	73.30 ± 0.02
	P3	15.72 ± 0.02	80.10 ± 0.15
BSA concentration (%w/w)	P4	36.07 ± 0.10	86.61 ± 0.01
	P5	52.0 ± 0.15	91.70 ± 0.02
Encapsulation time (h)	P6	14.83 ± 0.01	74.13 ± 0.01
	P7	14.98 ± 0.01	74.94 ± 0.01
	P8	15.23 ± 0.03	76.14 ± 0.15

Furthermore, the encapsulation time (3 h, 6 h, 12 h, and 24 h) affected % EE and %DL of BSA at constant weight ratio of (TMC and XG) (1:1) and [BSA]=25% (%w/w). The data illustrated that both % DL and % EE increased to 15.38% and 77.0% with an increase in encapsulation time at 24 h. The increase in the encapsulation time may led to a rise in the BSA loaded within PECs hydrogels chains through interaction forces.

Swell ability kinetic studies

The released protein from the polymer matrix is observed via the swelling behavior of the polymeric chains [49]. The kinetic swell ability of unloaded PEC (XG/TMC (1:1) in the absence of BSA was studied in pH 7.4 and pH 1.2 through time interval between 0.5 and 6 h at 37 °C. The data are shown in Fig. 7 showing that the swell ability of PEC hydrogels increases with the rise in the swelling time till equilibrium (attained after 4 h). Moreover, the PEC hydrogels swelling rate in pH 7.4 was higher than in pH 1.2. In acidic-buffered solution (pH 1.2), the electrostatic repulsion between protons and both hydroxyl and *N*-quaternized amino groups on hydrogel chains led to a reduction in their swelling rate. However, in slightly alkaline, pH 7.4, the –OH groups were ionized and extend repulsive forces with –COOH and *N*-methyl amino groups which led to an increase in the swelling rate % of PEC as it increased the counter ions concentrations within the polymer chains leading to the variance between the osmotic pressure of buffered solution inside and outside PEC hydrogels. The PEC hydrogels swelling ability balanced the rise in osmotic pressure [50].

BSA release

BSA released from BSA-loaded XG/TMC hydrogels was studied in two release media (pH 7.4 and 1.2) through various release times: between 12 and 120 h in the presence of various parameters such as polymer weight ratios (TMC: XG)

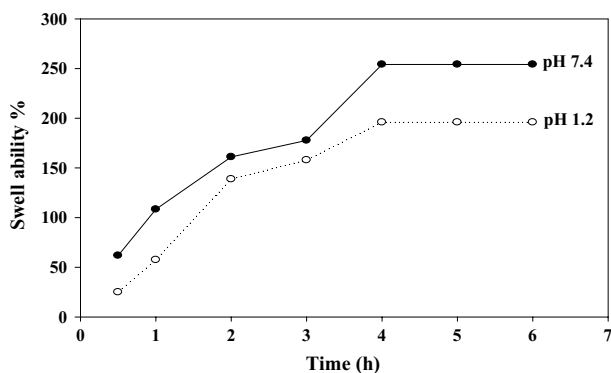


Fig. 7 Swell ability of PEC in pH 7.4 and pH 1.2 at different time periods 0.5–6 h

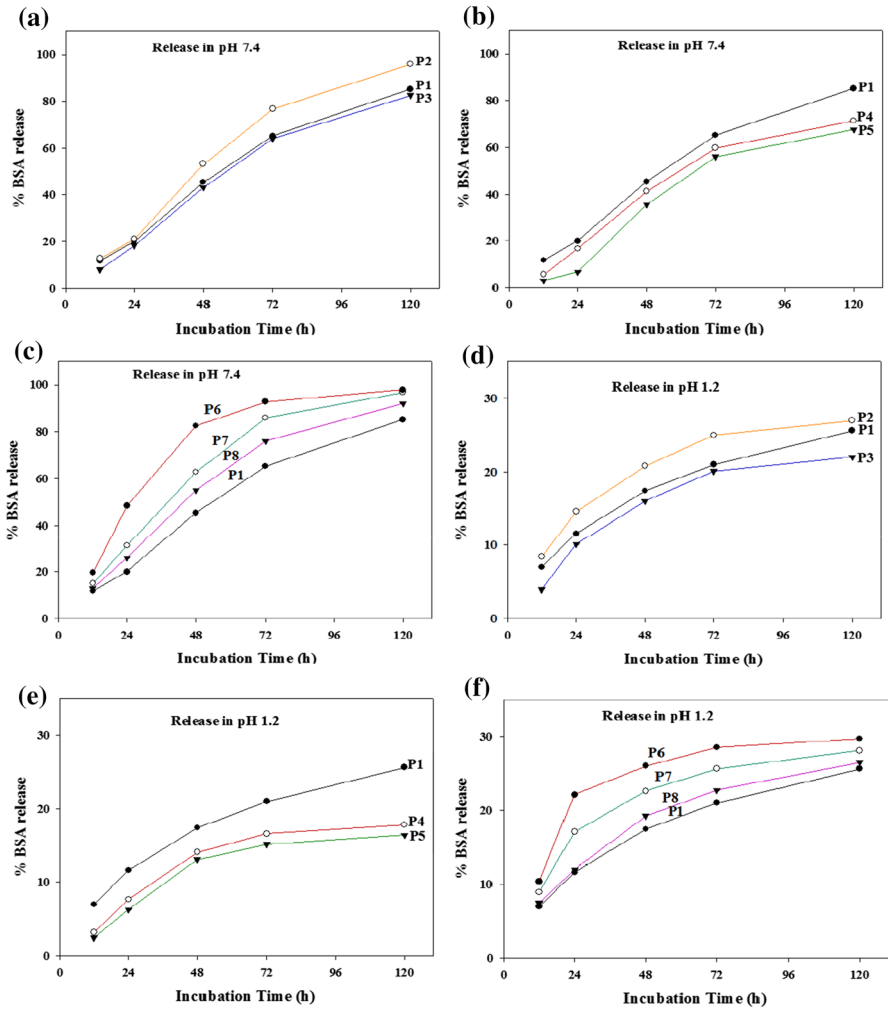


Fig.8 BSA accumulative release % from loaded matrixes in pH 7.4 and 1.2, release media, at various polymer weight ratios, different BSA concentrations and encapsulation times

(1:1) (P1), (1:2) (P2), and (2:1) (P3), different BSA-loaded concentrations: 25, 50, and 75% (w/w%) with codes P1, P4, and P5, respectively and different encapsulation times (3 h, 6 h, 12 h and 24 h with codes P6, P7, P8, and P1, respectively) at 37 °C. The data are shown in Fig. 8 illustrating the increase in BSA release rate out of the PECs hydrogels—in two media progressively—with the incubation time increase.

In addition, BSA release rate in pH 7.4 was faster than in pH 1.2 as the swelling behavior of PEC hydrogels. This observation was similar to BSA loading within modified glucomannan hydrogels [51]. The release rate relied on both dissolution and diffusion of the protein in the hydrogel [51].

Besides, the protein release from hydrophilic hydrogels counts on the matrix rigidity and its type [25]. The results of BSA release may be attributed to the increase in the electrostatic interactions in acidic medium (pH 1.2) that led to a reduction in BSA release [52, 53]. The isoelectric point of BSA is 4.8, thus at pH 7.4, the hydroxyl (-OH) groups along XG and TMC were ionized and BSA structure had negative net charges that led to an increase in the electrostatic repulsive forces between BSA and all ionized groups (-OH, -COO⁻ and *N*-mono and dimethyl amino groups) along PECs hydrogels and led to a rise in BSA release in pH 7.4. These results were similar to BSA release behavior in dextran hydrogels [54].

Effect of polymer weight ratios

The effect of (XG: TMC) weight ratios: (1:1) (P1), (1:2) (P2), and (2:1) (P3) was studied on BSA accumulative release from BSA/ PECs matrixes, keeping all other parameters constant (BSA concentration was 25% and encapsulation time was 24 h). BSA accumulative release went up with the increase in incubation time till reaching maximum value 85.2%, 95.9% and 82.6% in pH 7.4 and 25.6%, 27% and 22% in acidic (pH 1.2) medium for P1, P2 and P3, respectively. Data—(Fig. 8a and d)—exhibited that the increase in TMC content led to a reduction in BSA release from BSA-loaded hydrogel due to the increase in electrostatic interactions between TMC (*N*-quaternized amino groups) and carboxylic acid (-COOH) in BSA. This observation was similar to BSA released from loaded chitosan/poly(vinyl alcohol) hydrogels [47]

Effect of BSA concentration

The loaded BSA concentrations (25%, 50%, and 75%) affected the accumulative BSA release rate from PEC (XG: TMC) (1:1) at encapsulation time 24 h, and their codes, P1, P4, and P5 in both media (pH 7.4 and pH 1.2). The data are represented in Fig. 8b–e. When the BSA loaded increased from 25 to 75%, the BSA release decreased in pH 7.4 and pH 1.2 media. At 25%, the accumulative release was 85.2% in pH 7.4 and 25.6% in pH 1.2 in 120 h. While at 75%, BSA release was 67.7% in pH 7.4 and 16.4% in pH 1.2 in 120 h. The protein release % is monitored by its diffusion through the matrix and the relaxation process of the polymer upon solvent penetration [25]. Low protein loading (25%) on XG /TMC hydrogels formed a large pore led to good swelling that led to sharp BSA release in both release media. However, in the case of the high BSA loading (75%), the formation of strong interactions between BSA and polymer chains caused both reduction and shrinkage of the pores and cavities in BSA/PEC matrix led to the reduction in BSA release. This results were similar to other drugs release reported in the literature [25, 47, 55, 56].

Effect of encapsulation time

Encapsulation time (3 h, 6 h, 12 h and 24 h with codes P6, P7, P8 and P1, respectively) of loaded BSA (25%) within hydrogel (XG: TMC) (1:1%w/w) affected

accumulative BSA release % in pH 7.4 and 1.2 media, keeping all other parameters constant. The data are shown in Fig. 8c–f, showing that the increase in the encapsulation time led to decrease the accumulative BSA release % from interpolyelectrolyte complex. Because the increase in the encapsulation time resulted in filling both the pores and cavities along the interpolyelectrolyte complex surface with BSA as shown previously in SEM section that led to increase the interactions between loaded BSA and PEC structure, and then the free volume between PEC chains decreased that led to reduce the BSA accumulative release %. The encapsulation time 3 h (P6) showed high gradual BSA release till it reached maximum values 97.9% in pH 7.4 and 29.7% in pH 1.2 at 120 h. Reduction in BSA release as a result of the increase in encapsulation time has similar data reported in literature [25, 57].

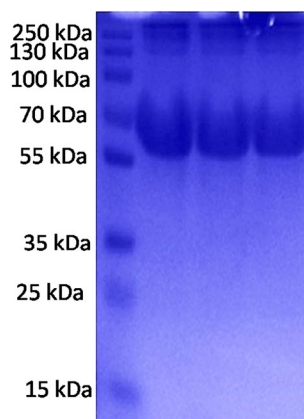
In vitro BSA release kinetic studies

In vitro BSA release from BSA/PECs hydrogels was studied kinetically in both pH 7.4 and pH 1.2 media in various incubation time intervals at 37 °C under the effect of various parameters: polymer weight ratios, different BSA concentrations and encapsulation times. The data are illustrated in Table 3 and fitted to Koresmeyer model. The mechanism of BSA release from the polymeric matrix in pH 7.4 and pH 1.2 followed non-Fickian model release since the diffusion exponent (*n*) values were ranging from 0.460 to 0.837. BSA release was affected by the blend of erosion and diffusion release-controlled. Moreover, the correlation coefficient (*R*²) values approached unity, suggesting the results were fitted to non-Fickian model. The data were similar to results of both BSA and diclofenac sodium release [29, 49, 58].

Table 3 Kinetic parameters: *R*² (correlation coefficient), *K* (rate constant) and *n* (diffusion exponent) of BSA release from loaded XG/ TMC PECs hydrogels

Sample code	Koresmeyer model							
	pH 7.4				pH 1.2			
	<i>R</i> ²	<i>k</i>	<i>n</i>	Release mechanism	<i>R</i> ²	<i>K</i>	<i>n</i>	Release mechanism
P1	0.9954	0.018	0.837	non-Fickian	0.9966	0.080	0.545	non-Fickian
P2	0.9910	0.010	0.575	non-Fickian	0.9991	0.114	0.475	non-Fickian
P3	0.9980	0.010	0.460	non-Fickian	0.9982	0.063	0.630	non-Fickian
P4	0.9927	0.006	0.784	non-Fickian	0.9447	0.010	0.768	non-Fickian
P5	0.9983	0.002	0.666	non-Fickian	0.9954	0.029	0.829	non-Fickian
P6	0.9999	0.035	0.699	non-Fickian	0.9999	0.046	0.695	non-Fickian
P7	0.9960	0.017	0.786	non-Fickian	0.9952	0.006	0.748	non-Fickian
P8	0.9943	0.012	0.626	non-Fickian	0.9865	0.071	0.589	non-Fickian

Fig. 9 SDS-PAGE method for examination of the structural integrity of BSA released in pH 7.4. Molecular marker (Lane 1), BSA standard (Lane 2), and BSA released out XG/TMC / BSA hydrogel into PBS medium after 24 h (Lane 3) and 120 h (Lane 4) of incubation



Detection of BSA structural integrity

The structural integrity of loaded BSA released out of PEC hydrogels into the release medium (pH 7.4) was examined with SDS-PAGE technique followed by staining with Coomassie brilliant blue, the results are shown in Fig. 9. The SDS-PAGE method is considered to be the principal method used for proteins separation according to the variances in their molecular weights [59]. In Fig. 9, the molecular weight markers and the BSA standard were observed in Lanes 1 and 2, respectively. The band was shown at 66 KDa, and the released BSA out of PEC into pH 7.4 medium through incubation time, 24 h and 120 h were observed in Lanes 3 and 4, respectively, as clear bands. Thus, these data confirmed that the loaded BSA was released in intact form out of the PECs, so the loaded BSA was not affected by both accumulation and destruction through its release from the PECs. From these results, we emphasize that the encapsulation and released conditions did not affect the integrity of BSA structure. These results were similar to other data mentioned in the literature [30, 60].

Cytotoxicity assays

Cytotoxicity assay is the significant analysis for choosing right vectors for the delivery of protein. For polymeric hydrogels to work as entire protein carriers, their composition must be non-toxic. The synthesized PEC cytotoxicity was checked versus HFB-4 (normal human melanocytes cells) employing the neutral red uptake assay. The cell viability % was measured and drawn versus various PEC hydrogel concentrations (Fig. 10).

The obtained results indicated that the examined XG/TMC PEC hydrogels showed the highest % cell viability $99.1\% \pm 2.5$ for $50 \mu\text{g/mL}$. The increase in PEC concentration to $300 \mu\text{g/mL}$ led to a decrease in the cell viability % to $88\% \pm 2.5$. It deduced the good biocompatibility for the examined PEC which can be used as a safe protein delivery system. These obtained results were similar to previous results reported in the literature [61].

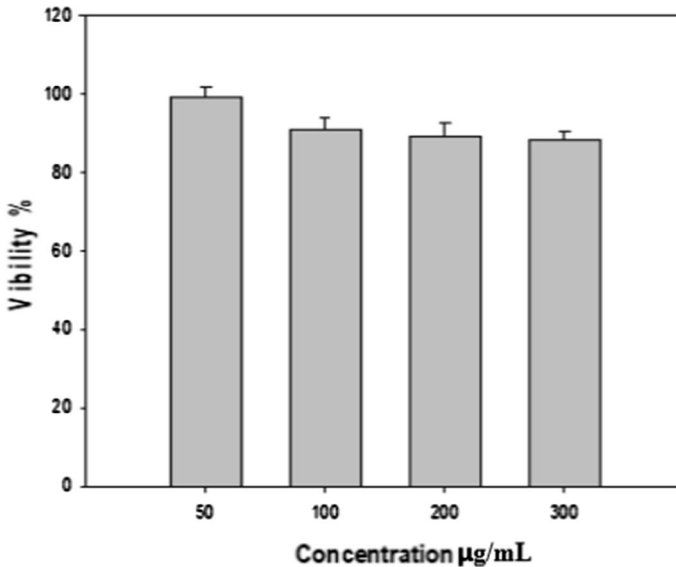


Fig.10 Cytotoxicity of the prepared PEC hydrogels using neutral red uptake assay

Conclusion

In the present study, polysaccharide gum as xanthan gum (XG) and trimethyl chitosan (TMC) (as two biodegradable polysaccharides) based PEC hydrogels were synthesized to encapsulate and deliver BSA successfully. The structure of PEC hydrogels in the absence/presence of BSA was elucidated with various analysis tools: FE-SEM, FTIR, EDX, and XRD.

The effect of various parameters such as, polymer weight ratios, different BSA concentrations and encapsulation time were examined to determine both DL% and EE % for BSA, also its *in-vitro* release out of loaded PEC in pH 7.4 and pH 1.2 buffered solutions.

The obtained results showed the increase in EE% with an increase in the encapsulation time, BSA concentration, and XG concentration. Moreover, the BSA release % in a slightly alkaline (pH 7.4) medium was faster than in acidic one, which increased with the increase in XG concentration where it reached maximum release value at XG: TMC (2:1) ratio and with the decrease in both BSA concentrations and encapsulation time.

In vitro BSA released mechanism was studied kinetically according to Korsmeyer model and the data illustrated that the mechanism followed non-Fickian mechanism in both media. Furthermore, the released BSA structure stability was confirmed with the SDS-PAGE assay and the obtained results exhibited that BSA structure released without any destruction.

Additionally, the cytotoxicity was examined for PEC sample against HFB-4 (normal human melanocytes cell line), and the obtained data represented that the prepared hydrogels can be applied as safe carriers for protein delivery.

References

1. Kang F, Singh J (2001) Effect of additives on the release of a model protein from PLGA microspheres. *AAPS PharmSciTech* 2(4):86–92
2. Okamoto MM, Anhê GF, Sabino-Silva R, Marques MFDSF, Freitas HS, Mori RCT, Melo KFS, Machado UF (2011) Intensive insulin treatment induces insulin resistance in diabetic rats by impairing glucose metabolism-related mechanisms in muscle and liver. *J Endocrinol* 211(1):55–64
3. Rubin RR, Peyrot M, Kruger DF, Travis LB (2009) Barriers to insulin injection therapy. *Diabetes Educ* 35(6):1014–1022
4. Sosnik A, Augustine R (2016) Challenges in oral drug delivery of antiretrovirals and the innovative strategies to overcome them. *Adv Drug Deliv Rev* 103:105–120
5. Ngwuluka NC, Abu-Thabit NY, Uwaezuoke OJ, Erebor JO, Ilomuanya MO, Mohamed RR, Soliman SM, Elella MHA, Ebrahim NA (2020) Natural polymers in micro-and nanoencapsulation for therapeutic and diagnostic applications: part I: lipids and fabrication techniques, nano-and microencapsulation-techniques and applications. IntechOpen, London
6. MacEwan SR, Callahan DJ, Chilkoti A (2010) Stimulus-responsive macromolecules and nanoparticles for cancer drug delivery. *Nanomedicine* 5(5):793–806
7. Li H, Zhang Z, Bao X, Xu G, Yao P (2018) Fatty acid and quaternary ammonium modified chitosan nanoparticles for insulin delivery. *Colloids Surf B* 170:136–143
8. Stopilha RT, Xavier-Júnior FH, De Vasconcelos CL, Fonseca JL (2020) Carboxymethylated- β -cyclodextrin/chitosan particles: bulk solids and aqueous dispersions. *J Dispersion Sci Technol* 41(5):717–724
9. Benny IS, Gunasekar V, Ponnusami V (2014) Review on application of xanthan gum in drug delivery. *Int J PharmTech Res* 6(4):1322–1326
10. Bejenariu A, Popa M, Dulong V, Picton L, Le Cerf D (2009) Trisodium trimetaphosphate crosslinked xanthan networks: synthesis, swelling, loading and releasing behaviour. *Polym Bull* 62(4):525–538
11. Kumar A, Rao KM, Han SS (2017) Application of xanthan gum as polysaccharide in tissue engineering: a review. *Carbohydr Polym* 180:128–144
12. Elella MHA, ElHafeez EA, Goda ES, Lee S, Yoon KR (2019) Smart bactericidal filter containing biodegradable polymers for crystal violet dye adsorption. *Cellulose* 26(17):9179–9206
13. Elella MHA, Sabaa M, Hanna DH, Abdel-Aziz MM, Mohamed RR (2020) Antimicrobial pH-sensitive protein carrier based on modified xanthan gum. *J Drug Deliv Sci Technol* 57:101673
14. Elella MHA, Goda ES, Gab-Allah MA, Hong SE, Pandit B, Lee S, Gamal H, Ur Rehman A, Yoon KR (2020) Xanthan gum-derived materials for applications in environment and eco-friendly materials: a review. *J Environ Chem Eng* 9:104702
15. Elella MHA, Goda ES, Abdallah HM, Shalan AE, Gamal H, Yoon KR (2021) Innovative bactericidal adsorbents containing modified xanthan gum/montmorillonite nanocomposites for wastewater treatment. *Int J Biol Macromol* 167:1113–1125
16. Xu T, Xin M, Li M, Huang H, Zhou S, Liu J (2011) Synthesis, characterization, and antibacterial activity of N, O-quaternary ammonium chitosan. *Carbohydr Res* 346(15):2445–2450
17. Muzzarelli RA, Tanfani F (1985) The N-permethylation of chitosan and the preparation of N-trimethyl chitosan iodide. *Carbohydr Polym* 5(4):297–307
18. Sadeghi AM-M, Dorkoosh F, Avadi M, Saadat P, Rafiee-Tehrani M, Junginger H (2008) Preparation, characterization and antibacterial activities of chitosan, N-trimethyl chitosan (TMC) and N-diethylmethyl chitosan (DEMC) nanoparticles loaded with insulin using both the ionotropic gelation and polyelectrolyte complexation methods. *Int J Pharm* 355(1–2):299–306
19. de Britto D, de Assis OB (2007) Synthesis and mechanical properties of quaternary salts of chitosan-based films for food application. *Int J Biol Macromol* 41(2):198–203
20. de Lima C, de Souza P, Stopilha R, de Morais W, Silva G, Nunes J, Wanderley Neto A, Pereira M, Fonseca J (2018) Formation and structure of chitosan–poly (sodium methacrylate) complex nanoparticles. *J Dispers Sci Technol* 39(1):83–91
21. de Lima C, de Morais W, Silva G, Nunes J, Neto AW, Pereira M, Fonseca J (2017) Preparation and characterization of dispersions based on chitosan and poly (styrene sulfonate). *Colloid Polym Sci* 295(6):1071–1078
22. de Britto D, Assis OB (2007) A novel method for obtaining a quaternary salt of chitosan. *Carbohydr Polym* 69(2):305–310

23. Chen X, Lv G, Zhang J, Tang S, Yan Y, Wu Z, Su J, Wei J (2014) Preparation and properties of BSA-loaded microspheres based on multi-(amino acid) copolymer for protein delivery. *Int J Nanomed* 9:1957
24. Yang J, Chen J, Pan D, Wan Y, Wang Z (2013) pH-sensitive interpenetrating network hydrogels based on chitosan derivatives and alginate for oral drug delivery. *Carbohydr Polym* 92(1):719–725
25. Ray R, Maity S, Mandal S, Chatterjee TK, Sa B (2010) Development and evaluation of a new interpenetrating network bead of sodium carboxymethyl xanthan and sodium alginate for ibuprofen release. *Pharmacol Pharm* 1(1):9
26. Long J, Yu X, Xu E, Wu Z, Xu X, Jin Z, Jiao A (2015) In situ synthesis of new magnetite chitosan/carrageenan nanocomposites by electrostatic interactions for protein delivery applications. *Carbohydr Polym* 131:98–107
27. Peppas N (1986) *Hydrogels in medicine and pharmacy, fundamentals, preparation method and structure of hydrogels*, vol I. CRS Press, Boca Raton, Florida
28. Bueno VB, Petri DFS (2014) Xanthan hydrogel films: Molecular conformation, charge density and protein carriers. *Carbohydr Polym* 101:897–904
29. Sahu SK, Prusty AK (2010) Design and evaluation of a nanoparticulate system prepared by biodegradable polymers for oral administration of protein drugs. *Die Pharmazie-An Int J Pharm Sci* 65(11):824–829
30. Laemmli UK (1970) Cleavage of structural proteins during the assembly of the head of bacteriophage T4. *Nature* 227(5259):680
31. Repetto G, Del Peso A, Zurita JL (2008) Neutral red uptake assay for the estimation of cell viability/cytotoxicity. *Nat Protoc* 3(7):1125
32. Salama HE, Saad GR, Sabaa MW (2016) Synthesis, characterization, and biological activity of cross-linked chitosan biguanidine loaded with silver nanoparticles. *J Biomater Sci Polym Ed* 27(18):1880–1898
33. Tian F, Liu Y, Hu K, Zhao B (2004) Study of the depolymerization behavior of chitosan by hydrogen peroxide. *Carbohydr Polym* 57(1):31–37
34. Rúnarsson ÖV, Malainer C, Holappa J, Sigurdsson ST, Másson M (2008) Tert-Butyldimethylsilyl O-protected chitosan and chitoooligosaccharides: useful precursors for N-modifications in common organic solvents. *Carbohydr Res* 343(15):2576–2582
35. Sajomsang W, Gonil P, Saesoo S (2009) Synthesis and antibacterial activity of methylated N-(4-N, N-dimethylaminocinnamyl) chitosan chloride. *Eur Polym J* 45(8):2319–2328
36. Avadi M, Sadeghi A, Tahzibi A, Bayati K, Pouladzadeh M, Zohuriaan-Mehr M, Rafiee-Tehrani M (2004) Diethylmethyl chitosan as an antimicrobial agent: synthesis, characterization and antibacterial effects. *Eur Polym J* 40(7):1355–1361
37. Mohamed RR, Elella MHA, Sabaa MW (2017) Cytotoxicity and metal ions removal using antibacterial biodegradable hydrogels based on N-quaternized chitosan/poly (acrylic acid). *Int J Biol Macromol* 98:302–313
38. Dai J, Yan H, Yang H, Cheng R (2010) Simple method for preparation of chitosan/poly (acrylic acid) blending hydrogel beads and adsorption of copper (II) from aqueous solutions. *Chem Eng J* 165(1):240–249
39. de Souza Costa-Júnior E, Pereira MM, Mansur HS (2009) Properties and biocompatibility of chitosan films modified by blending with PVA and chemically crosslinked. *J Mater Sci Mater Med* 20(2):553–561
40. Elella MHA, Mohamed RR, Abdel-Aziz MM, Sabaa MW (2018) Green synthesis of antimicrobial and antitumor N, N, N-trimethyl chitosan chloride/poly (acrylic acid)/silver nanocomposites. *Int J Biol Macromol* 111:706–716
41. Elella MHA, Mohamed RR, ElHafeez EA, Sabaa MW (2017) Synthesis of novel biodegradable antibacterial grafted xanthan gum. *Carbohydr Polym* 173:305–311
42. Mohamed RR, Elella MHA, Sabaa MW, Saad GR (2018) Synthesis of an efficient adsorbent hydrogel based on biodegradable polymers for removing crystal violet dye from aqueous solution. *Cellulose* 25(11):6513–6529
43. Sabaa MW, Hanna DH, Elella MHA, Mohamed RR (2019) Encapsulation of bovine serum albumin within novel xanthan gum based hydrogel for protein delivery. *Mater Sci Eng C* 94:1044–1055
44. Elella MHA, Sabaa MW, ElHafeez EA, Mohamed RR (2019) Crystal violet dye removal using crosslinked grafted xanthan gum. *Int J Biol Macromol* 137:1086–1101

45. Patel AS, Mishra P, Kanaujia PK, Husain SS, Prakash GV, Chakraborti A (2017) Investigating resonance energy transfer from protein molecules to van der Waals nanosheets. *RSC Adv* 7(42):26250–26255
46. Jian-feng G, Chang-jun H, Mei Y, Dan-qun H, Huan-bao F (2016) Ultra-sensitive fluorescence determination of chromium (VI) in aqueous solution based on selectively etching of protein-stabled gold nanoclusters. *RSC Adv* 6(106):104693–104698
47. Wang Q, Du YM, Fan LH (2005) Properties of chitosan/poly (vinyl alcohol) films for drug-controlled release. *J Appl Polym Sci* 96(3):808–813
48. Du J, Sun R, Zhang S, Govender T, Zhang LF, Xiong CD, Peng YX (2004) Novel polyelectrolyte carboxymethyl konjac glucomannan–chitosan nanoparticles for drug delivery. *Macromol Rapid Commun* 25(9):954–958
49. Bhattacharya SS, Ghosh AK, Banerjee S, Chattopadhyay P, Ghosh A (2012) Al³⁺ ion cross-linked interpenetrating polymeric network microbeads from tailored natural polysaccharides. *Int J Biol Macromol* 51(5):1173–1184
50. Soppimath KS, Kulkarni AR, Aminabhavi TM (2001) Chemically modified polyacrylamide-g-guar gum-based crosslinked anionic microgels as pH-sensitive drug delivery systems: preparation and characterization. *J Control Release* 75(3):331–345
51. Liu ZL, Hu H, Zhuo RX (2004) Konjac glucomannan-graft-acrylic acid hydrogels containing azo crosslinker for colon-specific delivery. *J Polym Sci Part A Polym Chem* 42(17):4370–4378
52. Liu WG, Li F, Zhao XD, Yao KD, Liu QG (2002) Atom force microscopic characterisation of the interaction forces between bovine serum albumin and cross-linked alkylated chitosan membranes in media of different pH. *Polym Int* 51(12):1459–1463
53. Li W, Xu R, Zheng L, Du J, Zhu Y, Huang R, Deng H (2012) LBL structured chitosan-layered silicate intercalated composites based fibrous mats for protein delivery. *Carbohydr Polym* 90(4):1656–1663
54. Schillemans JP, Hennink WE, van Nostrum CF (2010) The effect of network charge on the immobilization and release of proteins from chemically crosslinked dextran hydrogels. *Eur J Pharm Biopharm* 76(3):329–335
55. Rokhade AP, Agnihotri SA, Patil SA, Mallikarjuna NN, Kulkarni PV, Aminabhavi TM (2006) Semi-interpenetrating polymer network microspheres of gelatin and sodium carboxymethyl cellulose for controlled release of ketorolac tromethamine. *Carbohydr Polym* 65(3):243–252
56. Benita S, Barkai A, Pathak Y (1990) Effect of drug loading extent on the in vitro release kinetic behaviour of nifedipine from polyacrylate microspheres. *J Control Release* 12(3):213–222
57. Bhattacharya SS, Ghosh AK, Banerjee S, Chattopadhyay P, Ghosh A (2012) Al³⁺ ion cross-linked interpenetrating polymeric network microbeads from tailored natural polysaccharides. *Int J Biol Macromol* 51(5):1173–1184
58. Maiti S, Ray S, Sa B (2008) Effect of formulation variables on entrapment efficiency and release characteristics of bovine serum albumin from carboxymethyl xanthan microparticles. *Polym Adv Technol* 19(7):922–927
59. He Y, Yeung ES (2002) Rapid determination of protein molecular weight by the Ferguson method and multiplexed capillary electrophoresis. *J Proteome Res* 1(3):273–277
60. Li X, Kong X, Shi S, Zheng X, Guo G, Wei Y, Qian Z (2008) Preparation of alginate coated chitosan microparticles for vaccine delivery. *BMC Biotechnol* 8(1):89
61. Pakzad Y, Ganji F (2016) Thermosensitive hydrogel for periodontal application: in vitro drug release, antibacterial activity and toxicity evaluation. *J Biomater Appl* 30(7):919–929

Publisher's Note Springer Nature remains neutral with regard to jurisdictional claims in published maps and institutional affiliations.